

Quantum Control of Many-body Localized States

S. Choi,¹ N. Y. Yao,² S. Gopalakrishnan,¹ and M. D. Lukin¹

¹*Physics Department, Harvard University, Cambridge, Massachusetts 02138, USA*

²*Physics Department, University of California Berkeley, Berkeley, California 94720, USA*

(Dated: August 31, 2015)

We propose and analyze a new approach to the coherent control and manipulation of quantum degrees of freedom in disordered, interacting systems in the many-body localized phase. Our approach leverages a number of unique features of many-body localization: a lack of thermalization, a locally gapped spectrum, and slow dephasing. Using the technique of quantum phase estimation, we demonstrate a protocol that enables the local preparation of a many-body system into an effective eigenstate. This leads to the ability to encode information and control interactions without full microscopic knowledge of the underlying Hamiltonian. Finally, we analyze the effects of weak coupling to an external bath and provide an estimate for the fidelity of our protocol.

PACS numbers: 71.55.Jv, 05.30.Rt, 64.70.P-, 72.20.Ee, 71.23.An

The coherent control and manipulation of a complex quantum system is one of the central challenges of modern physics. The majority of ongoing research focuses on building up this complexity starting from individual, isolated qubits [1–7]. In contrast, the opposite approach, where one seeks the coherent manipulation of a strongly interacting system, especially subject to disorder, is generally thought to be intractable. The main difficulty is the exponentially growing Hilbert space with a typical many-body eigenstate strongly coupled to a dense set of other states. Even when the structure of relevant eigenstates is known, their many-body character generally makes them difficult to manipulate using most experimental controls.

In this Letter, we explore an alternate approach toward the coherent control of many-body systems. Our approach follows a new paradigm introduced by recent studies of many-body localization (MBL) [8–33]. In the presence of strong disorder, the many-body eigenstates of an isolated, interacting system can be localized in Fock space [13]. These MBL eigenstates exhibit a discrete local spectral response, suggesting that one can coherently manipulate and store quantum information (using external controls with both finite spatial and spectral resolution) [21, 22, 24]. This is remarkable because it implies that, in the presence of sufficiently strong disorder, local quantum bits naturally emerge from a strongly interacting many-body system [22, 25].

Further, in the MBL phase, these emergent qubits interact with one another via diagonal (i.e., dephasing) interactions; for two qubits separated by a distance d , this interaction time scales as $\sim \tau \exp(d/\xi)$, where τ is a characteristic timescale and ξ is the localization length [16, 20]. In this respect, the MBL phase differs crucially from, e.g., a conventional Anderson insulator, in which such interactions are absent [8, 14, 34]. This weak interaction brings about two implications for quantum control: (i) the coherence time of a single MBL qubit can be extremely long and (ii) dephasing can be leveraged

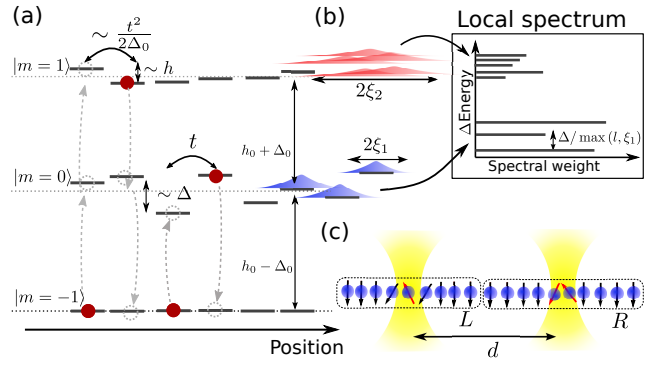


FIG. 1. (a) Schematic energy spectrum of the disordered spin-1 model. (b) A discrete local spectrum with excitations exhibiting different localization lengths. (c) External electromagnetic driving (yellow beam) defines the location of an MBL qubit.

as a way to coherently couple spatially separated MBL qubits [16]. Unfortunately, in general, the parametric dependence of both the coherence and dephasing times are identical. To make use of many-body localization as a platform for quantum control, one must devise a method to implement interactions (e.g. two-qubit quantum gates) on much shorter timescales than the decoherence.

Our approach relies upon three key ingredients. First, the local spectral gap of the MBL phase enables one to encode and manipulate quantum information using controls of both finite spatial and spectral resolution. Second, we demonstrate the ability to enhance interactions between MBL qubits by exploiting variations in the localization length of different eigenstates. Finally, we utilize quantum phase estimation and projective measurements to locally prepare the system in a many-body eigenstate ensuring that the interactions between spatially separated MBL qubits is coherent. In contrast to previous work [28], our approach uses the intrinsic dephasing interactions of the MBL phase as a resource to purify the

system. The combination of these ingredients can in principle, form the basis for a many-body localized quantum information processor. We find that such an approach can achieve a fidelity that asymptotically approaches the conventional method using isolated qubits. Perhaps more significantly, the local encoding of information provides new routes for studying and quantifying dynamics in the MBL phase. For example, one can imagine directly probing the decay of both the classical and quantum information, extracting the characteristic decay length for each [35], thereby gaining new insights into the nature of MBL systems.

Spin-1 model—To illustrate the key idea of our approach, we start with a simple model Hamiltonian that clearly exhibits two separate localization lengths. We will utilize excitations with a short localization length (“qubit” excitation) to encode information; meanwhile, to implement gates, we envision off-resonantly coupling such qubit excitations to a more delocalized excitation (“bus” excitation), thereby enhancing interactions on demand [4, 36].

Consider a chain of spin-1 particles with Hamiltonian,

$$H = \sum_{i=1}^N h_i S_i^z + \Delta_i (S_i^z)^2 + 2t \vec{S}_i \cdot \vec{S}_{i+1} \quad (1)$$

where N is the total number of sites (Fig. 1a). Disorder exists in both the magnetic field strength h_i and the single spin anisotropy Δ_i , which are randomly drawn from uniform distributions $[h_0 - h, h_0 + h]$ and $[\Delta_0 - \Delta, \Delta_0 + \Delta]$, respectively. As the Hamiltonian conserves total z -magnetization, $\sum_i S_i^z$, we can define a logical ground state $|G\rangle$ as the eigenstate with all spins in $|S_i^z = -1\rangle$. We focus on the regime in which the field disorder is much weaker than the anisotropy disorder, with a hierarchy,

$$t \ll h\Delta_0/\Delta \ll \Delta \ll \Delta_0 \lesssim h_0. \quad (2)$$

In this limit, there are two types of well-defined single-particle excitations. The first (qubit-type) consists of a single spin flipped into the $|S_i^z = 0\rangle$ state. This excitation moves in a disorder potential of strength Δ , analogous to Anderson localization [8]. As such, all single-particle states are localized and in the limit $t \ll \Delta$, the typical localization length of an excitation is given by $\xi_1^{-1} \sim \log \Delta/t$. The second single-particle excitation (bus-type) consists of a single spin flipped into the $|S_i^z = +1\rangle$ state; it can be regarded as a bound state of two qubit-type excitations, with binding energy $\sim \Delta_0$ (Fig. 1a). A bus excitation propagates via a second-order hopping process of amplitude $\sim t^2/(2\Delta_0)$. It, too, can be regarded as a localized single-particle excitation, with localization length, $\xi_2^{-1} \sim \log(h\Delta_0/t^2) = \xi_1^{-1} - \log[t\Delta/(h\Delta_0)]$. Under the hierarchy of equation (2), $\xi_2 \gg \xi_1$ (Fig. 1b).

We now turn to the case of multiple excitations. For sufficiently small t or sufficiently low energy densities,

the many-body eigenstates of this system are expected to exhibit many-body localization. The effective interaction between two excitations in the MBL phase falls off exponentially with distance; in the limit of low energy density, it is simply given by the overlap of their wavefunctions. Thus, for two qubit-type excitations a distance d from one another, the interaction strength is

$$\delta_I \sim t \exp(-d/\xi_1), \quad (3)$$

while for two bus-type excitations, the interactions scale as $\sim t \exp(-d/\xi_2)$.

Single qubit encoding and manipulation—In order to encode N_q qubits, we partition a given disordered system of size L into $N_q = L/d$ smaller segments of length $d > \xi_2 \gg \xi_1$. We select a single qubit-type excitation centered near the middle of each segment, and use it to encode the state of the MBL qubit (Fig. 1c). An arbitrary superposition of qubit states will dephase on a time scale $1/\delta_I$, and all gate operations must be fast compared to this timescale [16, 20].

The coherent manipulation of a single qubit state is feasible with local external control of finite spatial ℓ and spectral $\delta\omega$ resolution [24]. After initializing the system to the logical ground state $|G\rangle$, one applies a time-dependent electromagnetic field of frequency ω (Fig. 1c); to within exponentially small corrections, this transverse field couples $|G\rangle$ with only a finite number $\sim \max(\ell, \xi_1)$ of localized eigenstates, as depicted in Fig. 1b.

Thus, one can induce a high-fidelity transition between $|G\rangle$ and a specific eigenstate by weakly driving the system with ω tuned to the particular many-body transition ω_L . The requirements for the spatial and spectral resolution are: (i) $\ell < d$ and (ii) $\delta\omega < \Delta/\max(\ell, \xi_1)$. In this encoding scheme, information readout is performed by directly measuring the local spin polarization. In the limit $\xi_1 \rightarrow a$, this corresponds to the measurement of a single spin. When $\xi_1 > a$, the total polarization in the region determines the qubit state.

Two-qubit gates—To perform universal quantum control, we only need to demonstrate a controlled phase gate. As previously mentioned, such a gate can in principle, be achieved via the dephasing interactions of Eq. (3). However, since decoherence occurs at the same rate, one must effectively enhance this interaction strength. Since the dephasing between bus excitations occurs at a much faster rate te^{-d/ξ_2} , the effective interaction strength can be enhanced by several orders of magnitude upon dressing [37] a qubit-type excitation with a bus-type excitation. This enhancement ratio is given by,

$$\frac{\delta_I^{\text{driven}}}{\delta_I} \sim \frac{|\Omega|^2}{|\delta|^2} e^{d\left(\frac{1}{\xi_1} - \frac{1}{\xi_2}\right)} \quad (4)$$

where Ω is the Rabi frequency and δ is the detuning of the external driving field. A numerical demonstration of this enhancement in the simplified spin-1 model is provided in the Supplemental Material [38].

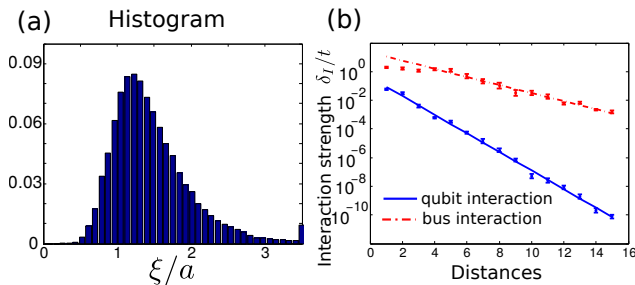


FIG. 2. Numerical study of localization lengths in the low spin density, weakly localized regime of Eq. (6). (a) Histogram of localization lengths in units of lattice spacing. Since the model conserves total S^z , one can choose to work in manifolds with a fixed density of excitations. Here, we consider two spin-flips. (b) Decay of the interaction strength as a function of distance for both qubit and bus excitations.

Generic MBL system—We now generalize our protocol from the spin-1 model to any MBL system with a fully localized spectrum [8–27]. Such systems can be represented in terms of conserved local spin-1/2 degrees of freedom termed “l-bits” [16, 20]:

$$H_{\text{mbl}} = \sum_i \bar{h}_i \tau_i^z + \sum_{i,j} \bar{J}_{ij} \tau_i^z \tau_j^z + \sum_{i,j,k} \bar{K}_{ijk} \tau_i^z \tau_j^z \tau_k^z \cdots \quad (5)$$

where the τ_i are spin-1/2 operators describing localized excitations of size ξ , \bar{h}_i is the energy of each excitation, \bar{J}_{ij} is the two-body interaction shift, etc. An l-bit overlaps with $\sim \xi$ microscopic degrees of freedom, and can therefore be individually addressed (up to exponentially small infidelities) using a drive with spectral resolution greater than $t/2\xi$. In addition, the l-bits have effective diagonal interactions that also fall off exponentially, with a localization length ξ that varies from site to site and (unlike the l-bit size ξ) from eigenstate to eigenstate [20]. All of the qualitative arguments from the spin-1 model extend to the generic case, provided (a) there are excitations that overlap spatially but have different localization lengths ξ , and (b) one can initially prepare the system in a particular eigenstate.

To understand the first of these issues, we numerically study the variation of localization lengths for the Hamiltonian,

$$H = \sum_i 2t \vec{S}_i \cdot \vec{S}_{i+1} + h_i S_i^z \quad (6)$$

where h_i is randomly drawn from a uniform distribution $[-\Delta, \Delta]$. This model is “generic” in that we have not engineered its localization lengths to have any particular features. In Fig. 2a, the histogram of localization lengths ξ is shown for low excitation density (up to two spin-flips) with weak disorder $\Delta/t = 3$ [38]. The distribution exhibits heavy tails, evincing the fact that there

is significant probability to find ξ longer than its average value. It turns out that variations always exist (even at high excitation densities) and are largest near the localization transition (see [38] for a quantitative analysis).

We note that our protocol does not require a parametric separation between long and short localization lengths; rather, one can optimize d to achieve as large an interaction enhancement as desired. To quantify the enhancement of the interaction strength, we numerically extract the localization length of typical qubit and bus excitations. We diagonalize systems up to length $L = 50$ with at most two excitations and perform 100 disorder averages. For each disorder realization, we a priori choose approximate positions for the left and right MBL qubits (at L and R). Starting from the polarized state $|G\rangle$, we identify computational qubits with significant local support around L, R . These basis states are chosen as energy eigenstates that have significant overlap with local excitation operators $\Sigma^{L(R)} = S_{L(R)-1}^x + S_{L(R)}^x + S_{L(R)+1}^x$. In particular, we select states $(\phi^L, \phi^R, \phi^{LR})$, such that $|\langle \phi^L | \Sigma^L | G \rangle|^2, |\langle \phi^R | \Sigma^R | G \rangle|^2, |\langle \phi^{LR} | \Sigma^L \Sigma^R | G \rangle|^2 > 10^{-2}$; moreover, to ensure that the MBL qubits are self-consistently defined, we require $|\langle \phi^{LR} | \Sigma^L | \phi^R \rangle|, |\langle \phi^{LR} | \Sigma^R | \phi^L \rangle| > 10^{-2}$.

This enables us to directly estimate the effective interaction between the MBL qubits from energy eigenvalues, with $\delta_I \equiv E_{LR} - E_L - E_R + E_G$. As the qubit(bus)-type excitation, we select basis states, $(\phi^L, \phi^R, \phi^{LR})$ that exhibit the smallest(largest) interaction strength [38]. As depicted in Fig. 2b, bus-type excitations interact significantly more strongly than qubit-type excitations, enabling multiple quantum gates to be performed within a decoherence window. While this simplified simulation does not account for the dynamical “dressing” of the qubits, the nature of the qualitative enhancement is the same: it comes from intrinsic variations of the many-body localization length (see [38] for full numerical simulations).

Initial state preparation—To enable fully coherent evolution, the interactions between MBL qubits must be coherent. This is indeed the case when the system is prepared in a fiducial many-body eigenstate; however, such a preparation is very difficult for a generic (high temperature) system. Since the MBL phase has a simple description in terms of local conserved quantities, each many-body eigenstate can be labeled by specifying the values (± 1) of all τ spins. The question is then: how can one efficiently prepare the system into a desired τ -spin superposition, starting from an arbitrary many-body state, with only local control over small sub-regions A and B . Let us label the two excitations L and R (in each region) to be our MBL qubits. The effective interaction between these qubits takes the form $\delta_I = J_{LR} + \sum_{k \notin \{A, B\}} K_{LkR} \tau_k + \dots$ for each τ -spin configuration [20]. Thus, starting from a generic many-body state, the effective interaction varies

from eigenstate to eigenstate and cannot enable a coherent quantum gate.

Interestingly, the interaction itself can be used as a resource to purify the entire system of τ -spins; in particular, by observing the interaction strength between the MBL qubits, one can effectively perform a quantum non-demolition measurement of the τ -spin configuration. Such an observation can be done via a modified spin-echo protocol [34], which projects the τ spins onto a set of configurations that have the same δ_I , up to the precision of the measurement.

Specifically, using an adaptive phase estimation algorithm [2, 28, 39], one can repetitively measure the interaction strength, $\delta_I = 2\pi t \sum_{\alpha=1}^M s_\alpha 2^{-\alpha}$ (in binary), to a precision set by its smallest significant digit s_M . To measure each digit, s_k , requires a time, $T_k = \frac{2^k}{t}$, yielding a total measurement time,

$$T_{tot} = \sum_{k=1}^M T_k = 2\tau_M(1 - 2^{-M}). \quad (7)$$

A few observations are in order: (1) this procedure is extremely efficient since the number of measurements M scales logarithmically with the desired precision and (2) the total measurement time T_{tot} is also the time-scale over which the MBL qubits can now be expected to interact coherently. This result implies that one can perform coherent quantum manipulations in the infinite temperature MBL phase with a preparation overhead scaling only linearly in time.

Imperfections—In what follows, we analyze a variety of realistic imperfections and provide a quantitative estimate for achievable fidelities in a number of experimental systems. In particular, we will consider the effect of finite spatial(ℓ) and spectral($\delta\omega$) resolution, leading to: (1) imperfect initialization, (2) off-resonant excitation, and (3) population loss into nearby modes.

For single qubit gates, the fidelity is given by,

$$\mathcal{F}_1 \simeq 1 - \frac{\ell}{\xi_1} \left(\frac{1}{T_2 \mathcal{E}} \right)^2, \quad (8)$$

where T_2 characterizes the extrinsic decoherence time and \mathcal{E} represents the local spectral gap. The lack of individual addressability manifests as a ratio of the spatial extent to the qubit localization length ℓ/ξ_1 , while off-resonant excitations induce an error $\sim 1/(T_2 \mathcal{E})^2$.

Turning to the fidelity for two qubit gates, we note that finite resolutions (spatial and spectral) bring about two consequences, namely, an optimal choice of qubit separation d_{opt} and a renormalized bus localization length $\xi_2 \rightarrow \xi_2^{eff}$ [38]. The former arises when the decoherence rate begins to dominate the bare interaction strength, while the latter occurs for line-widths larger than the local spectral gap. The physics of this latter case is analogous to coupling a single bound state (qubit excitation)

with a multi-particle continuum (bus excitation) of effective mass $m^* \simeq 1/ta^2$, and leads to a renormalized excitation size $\xi_2^{eff} \simeq a\sqrt{tT_2}$ [38, 40–42]. Combining these two effects gives an overall fidelity,

$$\mathcal{F}_2 \sim 1 - (t/\Gamma)^{-1+\xi_1/\xi_2^{eff}}, \quad (9)$$

where $\Gamma \simeq \ell^2/tT_2^2 a^2 + 1/T_2$ is an effective decoherence rate estimated from Fermi's Golden rule and $\xi_2^{eff} = \xi_2(\xi')$ for spectrally (un)-resolved bus excitations.

Interestingly, these bounds are consistent with traditional quantum information processing schemes based upon isolated qubits. In particular, for $\xi_1, \ell \rightarrow a$ and $\xi_2 \rightarrow \infty$, one discovers $\mathcal{F}_2^{opt} \simeq 1 - (tT_2)^{-1+\frac{1}{\sqrt{tT_2}}}$. This corresponds to two tightly localized qubits (e.g. atoms or bound states) interacting via a band of delocalized states (e.g. phonons or photons).

Fidelity Estimates—Our protocol applies most readily to quantum optical systems with local addressing. A number of such platforms are promising candidates for realizing many-body localization, including ultracold atoms, dipolar molecules, superconducting qubits, and solid-state spins [43–46]. In the case of ultracold atoms, a direct implementation of a spin system is feasible via multi-component Fermi- or Bose-Hubbard models. From recent experiments [47–49], the spatial resolution $\ell \sim a$, the typical superexchange interaction strength $t \sim 10\text{Hz}$, and the coherence limited by particle loss $T_2 \sim 3\text{s}$ are feasible, yielding an overall fidelity $\mathcal{F}_2 \approx 0.92$. Recent progress towards the engineering of large superconducting flux-qubit arrays is particularly intriguing [50, 51]; disorder naturally arises from the fabrication process and full tomography of the couplings within the system is daunting. Thus, the ability to define MBL qubits in a modular fashion is particularly applicable. With recent coherence times [52] $> 10\mu\text{s}$, typical interaction strengths $\sim 1\text{GHz}$, and individual flux-qubit control, one finds a fidelity $\mathcal{F}_2 \approx 0.99$. In the case of molecules and solid-state spin impurities, the interactions are long-range and the dominant disorder arises from random bonds. For effectively short-range power-laws, many-body localization persists and the main idea of this work is still applicable [26, 29, 30, 43].

In summary, we have introduced a scheme for the coherent control of local degrees of freedom in the many-body localized phase. Our approach enables encoding quantum information as well as to perform quantum logic between separated MBL qubits. This suggests that in certain cases, strongly disordered, interacting systems may be a resource for quantum information applications. The ability to efficiently prepare (high temperature) many-body eigenstates via local spectroscopy also opens the door to studying coherent dynamics in the MBL phase. By probing the decay of both classical and quantum information, it may be possible to characterize many-body localized states and their dynamics.

It is a pleasure to gratefully acknowledge the insights of and discussions with M. C. Banuls, A. Chandran, J. I. Cirac, E. Demler, A. V. Gorshkov, J. Haah, D. Huse, M. Knap, C. Laumann, V. Oganesyan, and A. Vishwanath. This work was supported, in part, by the Harvard-MIT CUA, the Kwanjeong Educational Fellowship, the AFOSR MURI, the ARO MURI, and the Miller Institute for Basic Research in Science.

-
- [1] T. D. Ladd, F. Jelezko, R. Laflamme, Y. Nakamura, C. Monroe, and J. L. O'Brien, *Nature* **464**, 45 (2010).
- [2] M. A. Nielsen and I. L. Chuang, (2010).
- [3] J. L. O'Brien, *Science* **318**, 1567 (2007).
- [4] H. Häffner, C. Roos, and R. Blatt, *Physics Reports* **469**, 155 (2008).
- [5] J. A. Jones, *Progress in Nuclear Magnetic Resonance Spectroscopy* **59**, 91 (2011).
- [6] D. Loss and D. DiVincenzo, *Phys. Rev. A* **57**, 120 (1998).
- [7] N. Y. Yao, L. Jiang, A. V. Gorshkov, P. C. Maurer, G. Giedke, J. I. Cirac, and M. D. Lukin, *Nature Communications* **3**, 800 (1).
- [8] P. W. Anderson, *Phys. Rev.* **109**, 1492 (1958).
- [9] D. M. Basko, I. L. Aleiner, and B. L. Altshuler, *Annals of Physics* **321**, 1126 (2006).
- [10] V. Oganesyan and D. Huse, *Phys. Rev. B* **75**, 155111 (2007).
- [11] M. Žnidarič, T. c. v. Prosen, and P. Prelovšek, *Phys. Rev. B* **77**, 064426 (2008).
- [12] A. Pal and D. A. Huse, *Phys. Rev. B* **82**, 174411 (2010).
- [13] C. Monthus and T. Garel, *Phys. Rev. B* **81**, 134202 (2010).
- [14] J. H. Bardarson, F. Pollmann, and J. E. Moore, *Physical Review Letters* **109**, 017202 (2012).
- [15] M. Serbyn, Z. Papić, and D. A. Abanin, *Phys. Rev. Lett.* **111**, 127201 (2013).
- [16] M. Serbyn, Z. Papić, and D. A. Abanin, *Phys. Rev. Lett.* **110**, 260601 (2013).
- [17] S. Iyer, V. Oganesyan, G. Refael, and D. Huse, *Phys. Rev. B* **87**, 134202 (2013).
- [18] Y. Bahri, R. Vosk, E. Altman, and A. Vishwanath, *arXiv.org* (2013), 1307.4092v2.
- [19] B. Bauer and C. Nayak, *Journal of Statistical Mechanics: Theory and Experiment* **2013**, P09005 (2013).
- [20] D. A. Huse, R. Nandkishore, and V. Oganesyan, *Physical Review B* **90**, 174202 (2014).
- [21] R. Nandkishore, S. Gopalakrishnan, and D. A. Huse, *Phys. Rev. B* **90**, 064203 (2014).
- [22] M. Serbyn, Z. Papić, and D. A. Abanin, *Phys. Rev. B* **90**, 174302 (2014).
- [23] N. Yao, C. Laumann, J. I. Cirac, M. Lukin, and J. Moore, *arXiv preprint arXiv:1410.7407* (2014).
- [24] A. Chandran, I. H. Kim, G. Vidal, and D. A. Abanin, *arXiv.org* (2014), 1407.8480v1.
- [25] R. Nandkishore and D. A. Huse, *arXiv.org* (2014), 1404.0686v2.
- [26] M. Pino, *arXiv.org* (2014), 1403.5974v1.
- [27] V. Khemani, R. Nandkishore, and S. L. Sondhi, *arXiv.org* (2014), 1411.2616v1.
- [28] B. Bauer and C. Nayak, *Phys. Rev. X* **4**, 041021 (2014).
- [29] A. L. Burin, *arXiv preprint cond-mat/0611387* (2006).
- [30] A. L. Burin, *Physical Review B* **91**, 094202 (2015).
- [31] V. Ros, M. Miller, and A. Scardicchio, *Nuclear Physics B* **891**, 420 (2015).
- [32] R. Vasseur, A. C. Potter, and S. A. Parameswaran, *Phys. Rev. Lett.* **114**, 217201 (2015).
- [33] A. C. Potter, R. Vasseur, and S. A. Parameswaran, *ArXiv e-prints* (2015), arXiv:1501.03501 [cond-mat.dis-nn].
- [34] M. Serbyn, M. Knap, S. Gopalakrishnan, Z. Papić, N. Y. Yao, C. R. Laumann, D. A. Abanin, M. D. Lukin, and E. A. Demler, *Phys. Rev. Lett.* **113**, 147204 (2014).
- [35] M.-C. Banuls *et al. in preparation*, .
- [36] This idea is analogous to the quantum information processing using trapped ions, where the interaction between ions(qubits) are mediated by photon(bus) modes.
- [37] M. Saffman, T. Walker, and K. Mølmer, *Reviews of Modern Physics* **82**, 2313 (2010).
- [38] Please, see Supplemental Material online.
- [39] G. Giedke, J. M. Taylor, D. D'Alessandro, M. D. Lukin, and A. Imamoglu, *Phys. Rev. A* **74**, 032316 (2006).
- [40] A. Goban, C. L. Hung, S. P. Yu, J. D. Hood, J. A. Muniz, J. H. Lee, M. J. Martin, A. C. McClung, K. S. Choi, D. E. Chang, O. Painter, and H. J. Kimble, *Nature Communications* **5**, 1 (1).
- [41] S. John and J. Wang, *Phys. Rev. B* **43**, 12772 (1991).
- [42] S. John and J. Wang, *Phys. Rev. Lett.* **64**, 2418 (1990).
- [43] N. Y. Yao, C. R. Laumann, S. Gopalakrishnan, M. Knap, M. Müller, E. A. Demler, and M. D. Lukin, *Phys. Rev. Lett.* **113**, 243002 (2014).
- [44] D. Basko, I. Aleiner, and B. Altshuler, *Phys. Rev. B* **76**, 052203 (2007).
- [45] B. Yan, S. A. Moses, B. Gadway, J. P. Covey, K. R. A. Hazzard, A. M. Rey, D. S. Jin, and J. Ye, *Nature* **501**, 521 (2013).
- [46] K. K. Ni, S. Ospelkaus, M. H. G. de Miranda, A. Pe'er, B. Neyenhuis, J. J. Zirbel, S. Kotochigova, P. S. Julienne, D. S. Jin, and J. Ye, *Science* **322**, 231 (2008).
- [47] N. Strohmaier, D. Greif, R. Jördens, L. Tarruell, H. Moritz, T. Esslinger, R. Sensarma, D. Pekker, E. Altman, and E. Demler, *Phys. Rev. Lett.* **104**, 080401 (2010).
- [48] S. Trotzky, P. Cheinet, S. Foelling, M. Feld, U. Schnorrberger, A. M. Rey, A. Polkovnikov, E. A. Demler, M. D. Lukin, and I. Bloch, *Science* **319**, 295 (2008).
- [49] T. Fukuhara, *Nature Physics* **9**, 235 (2013).
- [50] M. W. Johnson, M. H. S. Amin, S. Gildert, T. Lanting, F. Hamze, N. Dickson, R. Harris, A. J. Berkley, J. Johansson, P. Bunyk, E. M. Chapple, C. Enderud, J. P. Hilton, K. Karimi, E. Ladizinsky, N. Ladizinsky, T. Oh, I. Perminov, C. Rich, M. C. Thom, E. Tolkacheva, C. J. S. Truncik, S. Uchaikin, J. Wang, B. Wilson, and G. Rose, *Nature* **473**, 194 (2011).
- [51] T. Lanting, A. J. Przybysz, A. Y. Smirnov, F. M. Spedalieri, M. H. Amin, A. J. Berkley, R. Harris, F. Altomare, S. Boixo, P. Bunyk, N. Dickson, C. Enderud, J. P. Hilton, E. Hoskinson, M. W. Johnson, E. Ladizinsky, N. Ladizinsky, R. Neufeld, T. Oh, I. Perminov, C. Rich, M. C. Thom, E. Tolkacheva, S. Uchaikin, A. B. Wilson, and G. Rose, *Phys. Rev. X* **4**, 021041 (2014).
- [52] M. Stern, G. Catelani, Y. Kubo, C. Grezes, A. Bienfait, D. Vion, D. Esteve, and P. Bertet, *Phys. Rev. Lett.* **113**, 123601 (2014).

Supplemental Material for Quantum Control of Many-body Localized States

S. Choi, N. Y. Yao, S. Gopalakrishnan, M. D. Lukin

Numerical methods and details—Here, we provide full numerics for our protocol in both the spin-1 model in Eq. (1) and the generic Heisenberg spin-1/2 model with random fields (Eq. 9). The general outline of the demonstration is the following. First, for a given realization of a disordered Hamiltonian we numerically identify two qubit- and bus-type excitations, located at positions L and R . Second, we compute the effective interaction strength between qubits either with or without off-resonant coupling to the bus excitations. Third, we repeat this process for various distances separating L and R and average the interaction strength over 500 realizations. Below, we provide the details of this process for both spin-1 and spin-1/2 models, always setting the lattice spacing $a = 1$.

For the spin-1 model, we exactly diagonalize a system of 14 spins (Eq. 1) with $\Delta_0 = 25, \Delta = 15, h_0 = h = 0.02$, and $t = 1$. The Hamiltonian conserves total z -magnetization, $\sum_i S_i^z$. Therefore, we only need to diagonalize a few relevant symmetry sectors of the Hilbert space, namely, systems with up to four spin excitations starting from the spin polarized state $|G\rangle$. A single qubit excited state at position i is identified as the energy eigenstate with the largest overlap with $S_i^x |G\rangle$ where S_i^x is the spin flip operator at position i . We denote the eigenstate with a single excitation at position L as $|\phi^L\rangle$. In this simulation we choose $L = 3$. Similarly, we identify eigenstates with single qubit excitations at various positions $R = 8, 9, 10, 11$, and 12th site and denote them as $|\phi^R\rangle$. The eigenstates with two qubit excitations $|\phi^{LR}\rangle$ and bus excitations at L (or R) are also identified in a similar way from $S_R^x |\phi^L\rangle$ and $S_L^x |\phi^L\rangle$ (or $S_R^x |\phi^R\rangle$), respectively. The off-resonant driving on the left qubit has been implemented by transforming the Hamiltonian into the rotating frame with a rotating wave approximation. The time-dependent driving on the right qubit has been numerically integrated over one period, and then the long time dynamics is studied in the Floquet basis. As discussed in the main text, the effective interaction strength between the MBL qubits is directly calculated from energy eigenvalues,

$$\delta_I \equiv E_{LR} - E_L - E_R + E_G. \quad (\text{S1})$$

This is also the case for the driven hamiltonian in the Floquet basis, where energies are defined via logarithms of unitary evolution. The average interaction strength as a function of distance is shown in Fig. S1a. We confirm the exponential decay of the bare interaction strength δ_I with a length scale $\xi_1 \approx 0.53$ (blue solid line), which agrees with our simple theoretical estimate $(\log \frac{\Delta}{t})^{-1} \approx 0.5$. When the qubits are driven, the interaction is enhanced by several orders of magnitude (red dash-dot line and green dotted line). Moreover, we observe that the enhanced interaction strength scales quadratically in Ω/δ (see Fig. S1b), confirming the off-resonant dressing picture presented in Eq. (7) of the main text.

We use a similar technique to simulate a system of 16 spins in the Heisenberg model, with $t = 1$ and $\Delta = 7.5$. Again, the simulation supports up to four excitations from the polarized state $|G\rangle$. Unlike our spin-1 model, the qubit excitations are identified by their energy eigenvalues; single spin excitations with the highest and the lowest energies are used as $|\phi^L\rangle$ and $|\phi^R\rangle$ depending on their relative positions. A single excitation with either high or low energy is expected to have a short localization length. Therefore, coupling to any subsequent excitations will, on average, enhance the effective interaction. Note that our criteria of identifying qubit- and bus-excitations can be

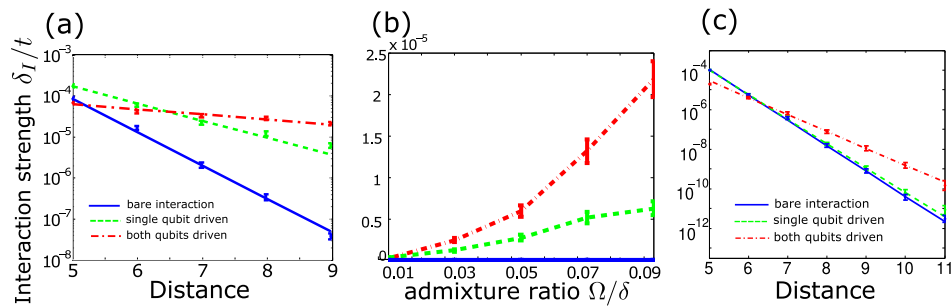


FIG. S1. Effective interaction strength. (a) Interaction strength decays more weakly when either one or both qubits are off-resonantly coupled to the bus excitations. (b) The enhanced interaction strength is quadratic in the ratio of Rabi frequency to detuning Ω/δ as expected for off-resonant dressing. (c) Effective interaction strength decay for the random field Heisenberg model.

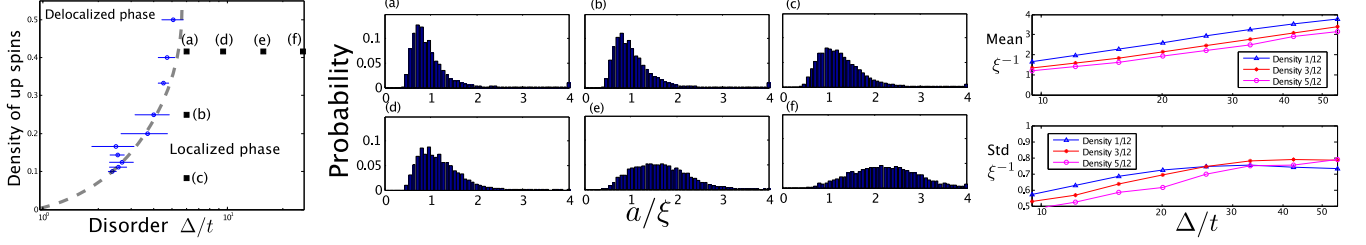


FIG. S2. Variation in the localization lengths. Left: the phase diagram of the random field Heisenberg spin-1/2 model as a function of spin density and disorder. Middle: histograms of the inverse localization length for parameters shown in the left panel. Right: mean and standard deviation of the inverse localization length in the strong disorder regime.

further optimized to achieve a stronger interaction enhancement. We estimate the positions of qubit excitations $p_{L(R)}$ by maximizing $|\langle \phi^{L(R)} | S_{p_{L(R)}}^x | G \rangle|$, and then identify bus excitations from $S_{p_{L+1}}^x | \phi^L \rangle$ and $S_{p_{R-1}}^x | \phi^R \rangle$, i.e. nearest subsequent excitations. The effective interaction strength as a function of distance is shown in Fig. S1c. Again, we confirm that the enhancement is exponentially large at long distances. We emphasize that this model does not have ‘engineered’ localization lengths as in the spin-1 model.

The typical localization lengths of qubit and bus excitations can be obtained from the slopes in Fig. S1c, yielding $\xi_1 \sim 0.34$ (blue solid line) and $\xi_2 \sim 0.50$ (red dash-dot line). These values are consistent with the probability distribution of localization lengths studied in the next section.

Variation of localization lengths—Here, we provide numerics showing that a variation in localization lengths always exists in the localized phase of the random field Heisenberg model (this variation is of course most pronounced near the transition).

First, to work in the localized phase, we estimate the critical disorder Δ/t for the many-body localization phase transition for various spin excitation densities (relative to the polarized state $|G\rangle$). We follow the method used in Ref. [1], and calculate the fraction of dynamical polarization at infinite temperature. The result is summarized in the left panel of Fig. S2. We confirm that the transition occurs at $\Delta/t \sim 5$ for high densities, consistent with previous results for small system sizes [1]. At low densities, the critical disorder is smaller, approaching the limit of the Anderson localization criteria in 1D $\Delta/t \rightarrow 0$.

We study the variation of localization lengths under various conditions. Here, we *define* the localization length of excitations with respect to a particular many-body eigenstate in the following way. First, we exactly diagonalize a system of 12 spins, choosing an arbitrary energy eigenstate with total spin up density $n_s = \sum_i \langle (S_i^z + \frac{1}{2}) \rangle / N$ and define it as our logical ground state $|\mathcal{G}\rangle = |00\rangle$. Then, we choose two ‘probing positions’ $L_p = 2$ or 4 and $R_p = 9$ or 11 and identify all possible computational basis states (*viz.* $|01\rangle$, $|10\rangle$, and $|11\rangle$) as energy eigenstates that have large enough overlap with $S_R^+ |00\rangle$, $S_L^+ |00\rangle$, and $S_L^+ S_R^+ |00\rangle$; we also impose that these states satisfy the consistency condition $|\langle 11 | S_L^+ |01\rangle|, |\langle 11 | S_R^+ |10\rangle| > c$ with a threshold $c = 0.01$. The relative differences in the energy eigenvalues of these states *defines* the interaction strength δ_{int} and the localization length ξ by

$$d/\xi \equiv -\log\left(\frac{|\delta_{\text{int}}|}{t}\right) = -\log\left(\frac{|E_{11} - E_{10} - E_{01} + E_{00}|}{t}\right) \quad (\text{S2})$$

where E_{ab} is the energy eigenvalue for $|ab\rangle$ and the distance between two excitations d is computed in the same way as in the previous section. We repeat this process for different logical ground states and disorder realizations; various values of n_s and Δ/t are shown as black squares (a-f) in Fig. S2(left). For each case, the histogram of inverse localization lengths is shown in the middle panel of Fig. S2. Note that we have chosen to histogram $1/\xi$ rather than ξ because the Jacobian induces long tails in ξ .

The mean of the inverse localization length increases with both decreasing spin density and increasing disorder strength. It may seem that the variance of the distribution is also increasing with disorder strength in (a), (d), (e), and (f); however, this behavior does not continue at larger disorder strengths. Rather, as shown in the right panel of Fig. S2, the standard deviation saturates near $\Delta/t \sim 30$ while the mean continues to increase.

Initialization and DEER sequences— Here, we provide the detailed protocol for initializing the system into an effective many-body eigenstate using a combination of DEER (double electron electron resonance) spin echo and efficient quantum phase estimation [2, 3]. We assume that the quantum state of the system is initially in an unknown

superposition of many-body eigenstates. Our goal is to efficiently prepare a quantum state such that the coherence of qubit excitations and their interactions is maintained for sufficiently long times. In doing so, we only use local operators and projective measurements limited to the accessible region of size ℓ . We assume that we can start by preparing the small local regions $L(R)$ into their respective local eigenstates $|0_{L(R)}\rangle$ (e.g. eigenstates of τ^z spin operators within the region) [4].

The state of the full system can be written in the τ^z basis as

$$|\psi_0\rangle = \sum_M c_M |0_L\rangle \otimes |M\rangle \otimes |0_R\rangle \quad (\text{S3})$$

where M enumerates all (exponentially many) possible configurations for the uninitialized regions. Then, we perform local spectroscopy in each region (L and R) in order to estimate the energy of a single excitation at the center of the region. Due to the diagonal interactions in the MBL phase, the spectral lines for these excitations are broadened by at most $\sim t \exp(-l/\xi_2)$. With $\ell \gg \xi_2$, one can resolve and manipulate individual localized excitations in each region within a timescale $\sim t^{-1}$. We choose a single excitation in each region to use as our MBL qubits. These qubit excitations interact with spins in the rest of the chain and therefore dephase over a time scale $T \sim t^{-1} \exp(\ell/\xi_2)$. This dephasing can in principle be refocused by the spin echo sequence considered in Fig. S3a [2].

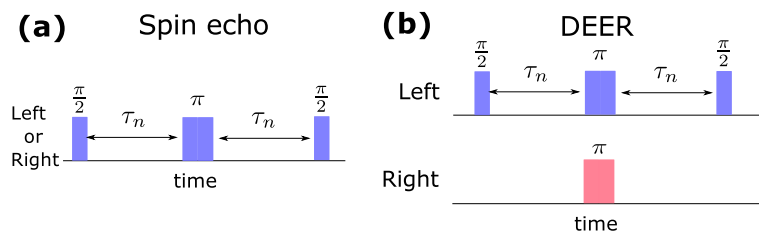


FIG. S3. Spin echo pulse sequences. (a) The dephasing of the left MBL qubit can be refocused via a simple Hahn echo. (b) a modified spin echo sequence (DEER) isolates the dephasing of the left MBL qubit induced by interactions $\delta_I = \delta_{LR} + \delta_{LMR}$.

For coherent interactions between MBL qubits, one needs to further initialize the system, since the interaction strength δ_I depends on the configuration M of the uninitialized region. For a specific M , the interaction can be written as $\delta_I = \delta_{LR} + \delta_{LMR}$ [4]. Here, one can understand δ_{LR} as the direct interaction between the two excitations while δ_{LMR} is the contribution provided by all of the multi-body interactions mediated by τ -spins in the uninitialized region. It is this dependence of δ_I on M that prevents the coherent interaction between MBL qubits [2]. Interestingly, this problem can be solved by precisely measuring δ_I (to within $\delta\omega$) since the measurement serves as a quantum non-demolition measurement for the configuration of the uninitialized region. Note that this simple solution is only possible due to the lack of thermalization in the MBL phase.

For the measurement of δ_I , we consider a modified spin echo sequence, known as DEER, as depicted in Fig. S3b [2]. This sequence refocuses the dephasing of the left MBL qubit induced by all but the MBL qubit on the right [2]. Each measurement of δ_I projects the many-body state of the system into a superposition of a few eigenstates that share the values of δ_I consistent with the measurement outcomes. Note that we do *not* require the preparation of a unique eigenstate as long as the prepared state enables coherent interactions between MBL qubits up to a desired time scale $T \sim \delta\omega^{-1}$. Repeating the DEER sequence (followed by measurements of the left MBL qubit) with a free evolution time τ_n measures the phase shift $\delta_I \tau_n$ modulo 2π . Therefore, by varying the free evolution time $\tau_n = 2^{-n}/\delta\omega$ with $n = 0, 1, 2, \dots$, one can efficiently measure δ_I up to the desired precision $\delta\omega$ [3]. This particular sequence of τ_n is chosen such that the protocol minimizes the total evolution time and is well described in Ref. [3]. The total measurement time $\sum \tau_n$ scales linearly with the inverse of the desired resolution $T_{\text{init}} = \eta\delta\omega$, where a constant of order unity $\eta > 2$ accounts for the repetition of the $n = 0$ step due to projection noise.

Fidelity estimates— Here, we analyze the fidelity of single qubit and gates under various conditions. The single qubit fidelity depends on both (i) whether the broadened spectral lines have power-law tails (e.g., a Lorentzian) or fall off more rapidly (e.g., a Gaussian) and (ii) how the spatial resolution ℓ compares with ξ_1 . When $\ell \lesssim \xi_1$, local level repulsion ensures that there are no levels within the local spectral gap \mathcal{E} of the targeted level that couple to the external driving field; when $\ell > \xi_1$, approximately $\delta\omega/\mathcal{E}$ levels per localization length are within the spatial extent of the driving, where $\delta\omega \sim 1/T_2$ is the spectral resolution. Moreover, when the linewidth is Lorentzian, the dominant imperfections are due to nearby transitions that use the tails $\sim (\delta\omega/\mathcal{E})^2$ of the Lorentzian (spectral imperfection);

$1 - \mathcal{F}_1$	Gaussian	Lorentzian
$l < \xi_1$	$\exp[-2\mathcal{E}/\delta\omega]$	$(\delta\omega/\mathcal{E})^2$
$l > \xi_1$	$(l/\xi_1) \times (\delta\omega/\mathcal{E})$	$(l/\xi_1) \times (\delta\omega/\mathcal{E})$

TABLE I. Fidelity of one-qubit gates for finite spectral and spatial resolution under various conditions. Two different types of spectral profiles arise from different origins: Gaussian from inhomogeneous broadening, including the effects of the bare un-enhanced interaction, and Lorentzian from homogeneous broadening, e.g., extrinsic decoherence processes.

whereas, for rapidly decaying tails, the dominant imperfections are due to distant, exponentially weak lines that are within $\delta\omega$ of the targeted line (spatial imperfection). Fidelities in the four cases are summarized in Table I.

We now focus on the fidelity of two qubit gates and derive Eq. (12) in the main text, which we present here again for convenience,

$$\mathcal{F}_2 \simeq 1 - (t/\Gamma)^{-1+\xi_1/\xi_2^{eff}} \quad (S4)$$

where Γ is an effective decoherence rate and ξ_2^{eff} is an effective localization length for bus excitations.

In general, the fidelity of a two qubit gate is given as

$$1 - \mathcal{F}_2 \simeq \frac{\max(\Gamma, \delta_I)}{\delta_I^{\text{driven}}} \quad (S5)$$

where the numerator is the rate of decoherence due to either external imperfections or bare dephasing interactions, while the denominator is the strength of the enhanced interaction. One can always optimize d such that $\delta_I(d_{\text{opt}}) = \Gamma$. Then, using $\delta_I^{\text{driven}} \sim t e^{-d_{\text{opt}}/\xi_2^{eff}}$, one can obtain Eq. (12). The dominant contributions to Γ and ξ_2^{eff} vary under differing conditions. First, ξ_2^{eff} is either ξ_2 or $\xi' \approx a\sqrt{tT_2}$ depending on the spectral resolution. When $1/T_2$ is larger than the typical energy spacing of bus-type excitations \mathcal{E}_2 , one necessarily couples a single MBL qubit with multiple excitations. In this case, the spatial extent of the qubit is broadened in the same way as that of a bound state coupled to a multi-particle continuum of effective mass $m^* \approx 1/ta^2$, leading to $\xi' \approx \sqrt{T_2/m^*} \approx a\sqrt{tT_2}$ [5–7]. The effective decoherence rate Γ is limited by the rate of population loss as well as the extrinsic decoherence scale, $\Gamma = \max(\Gamma_{\text{loss}}, 1/T_2)$, where Γ_{loss} can be estimated using Fermi's golden rule

$$\Gamma_{\text{loss}} \sim \frac{1/T_2}{1/T_2^2 + \Delta^2} \left(\frac{l}{\xi_2} \Omega \right)^2 \frac{\Delta}{\mathcal{E}_2}. \quad (S6)$$

The first factor comes from the Lorentzian spectrum, the second from the effective coupling strength, and the last from the density of bus excitation states. In order to maximize the size of the dressed qubit, Δ needs to be as small as possible, limited only by $1/T_2$. Therefore, we set $\Gamma \sim 1/(T_2^2 \mathcal{E}_2) (l/\xi_2)^2$, wherein the corresponding optimal spacing is given by $d_{\text{opt}} = \xi_1 \ln [tT_2 \min(1, T_2 \mathcal{E}_2 \xi_2^2/l^2)]$. There is a cross over at $l^2/T_2 = \mathcal{E}_2 \xi_2^2$; when $l^2/T_2 > \mathcal{E}_2 \xi_2^2$ the loss error limits the fidelity, and d_{opt} has to be relatively small in order to avoid long gate operation times. For $l^2/T_2 < \mathcal{E}_2 \xi_2^2$, the spectral lines of the bus-excitations are not resolved, but the fidelity remains limited by the number of gate operations within a decoherence window. Thus, one finds

$$1 - \mathcal{F}_2 \simeq (tT_2)^{-1+\xi_1/\xi'}. \quad (S7)$$

We can estimate the fundamental limit of our protocol by considering a system optimized for our purposes viz. a system that supports different types of excitations with $\xi_2/\xi_1 \rightarrow \infty$ with perfect spatial resolution and finite decoherence time $T_2 < \infty$. In this case the optimal fidelity is achieved from Eq. (S7). Consequently, in the limit $\xi_2 \rightarrow \infty$ and $\xi_1 \rightarrow a$, we obtain $\mathcal{F}_2^{\text{opt}} \simeq 1 - (tT_2)^{-1+\frac{1}{\sqrt{tT_2}}}$ as presented in the main text.

-
- [1] A. Pal and D. A. Huse, Phys. Rev. B **82**, 174411 (2010).
[2] M. Serbyn, M. Knap, S. Gopalakrishnan, Z. Papić, N. Y. Yao, C. R. Laumann, D. A. Abanin, M. D. Lukin, and E. A. Demler, Phys. Rev. Lett. **113**, 147204 (2014).
[3] G. Giedke, J. M. Taylor, D. D'Alessandro, M. D. Lukin, and A. Imamoglu, Phys. Rev. A **74**, 032316 (2006).
[4] D. A. Huse, R. Nandkishore, and V. Oganesyan, Physical Review B **90**, 174202 (2014).
[5] A. Goban, C. L. Hung, S. P. Yu, J. D. Hood, J. A. Muniz, J. H. Lee, M. J. Martin, A. C. McClung, K. S. Choi, D. E. Chang, O. Painter, and H. J. Kimble, Nature Communications **5**, 1 (1).
[6] S. John and J. Wang, Phys. Rev. B **43**, 12772 (1991).
[7] S. John and J. Wang, Phys. Rev. Lett. **64**, 2418 (1990).